Apoptosis Triggering in Breast Cancer Cells with Co-delivery of Melatonin and Doxorubicin Loaded into Human Adipose Mesenchymal Stem Cell Derived Exosomes

Moein Shirzad
Babol University of Medical Science
Abdolreza Daraei
Babol University of Medical Science
Hossein Najafzadehvarzi
Babol University of Medical Science
Nazila Farnoush
Babol University of Medical Science
Hadi Parsian
hadiparsian@mubabol.ac.ir

Babol University of Medical Science https://orcid.org/0000-0002-3965-7566

Research Article

Keywords: Extracellular vesicles (EVs), Exosomes (EXOs), Mesenchymal stem cells (MSCs), Doxorubicin (DOX), Melatonin (MEL), Breast cancer

Posted Date: April 3rd, 2024

DOI: https://doi.org/10.21203/rs.3.rs-3906438/v1

Abstract

Background

In recent years, numerous efforts have been dedicated to reducing the side effects of doxorubicin (DOX). Exosomes (EXOs), as extracellular vesicles (EVs), can play a role in the safe transport of DOX in breast cancer treatment. The aim of this study was to alleviate the adverse effects associated with DOX while enhancing its targeted delivery to cancer cells through the codelivery of melatonin (MEL) as an antioxidant and DOX into EXOs-derived from human adipose tissue mesenchymal stem cells (A-MSCs).

Methods

MSCs were isolated from liposuction samples using collagenase II enzyme, and stemness markers were evaluated by flow cytometry. EXOs were extracted from conditioned A-MSCs media through ultracentrifugation, and surface markers were evaluated by western blotting, DLS and TEM. The absorption and release of EXOs in cells were investigated using PKH-26 dye and UV–Vis spectrophotometry, respectively. DOX and MEL were loaded into EXOs using the sonication method, and their cytotoxic effects on normal and cancer cells were evaluated using the MTT test. Additionally, the expression of p53, NANOG, and miR-34a genes was analyzed using qRT-PCR, and apoptosis was assessed using flow cytometry and acridine/orange dye.

Results

It was observed that they exhibited remarkable stability under pH ~ 7.4 while displaying a high release rate under low pH conditions commonly found within cancerous environments (pH ~ 5.0). Cellular uptake experiments revealed a substantial percentage of internalization. Cytotoxicity evaluation demonstrated that co-delivery of DOX and MEL into EXOs (Exo-DOX-MEL) enhanced their toxicity towards normal MCF-10A and A-MSC cells, while exhibiting greater lethality towards MCF-7 and MDA-MB231 cancer cells. In normal cells, Exo-DOX-MEL augmented the effects of DOX, leading to increased expression of p53 and miR-34a and decreased expression of NANOG, particularly in MCF-7 and MDA-MB231 cells. Apoptotic analysis validated the favorable outcomes associated with Exo-DOX-MEL, which enhanced DOX efficacy in cancer cells while reducing apoptosis in normal cells compared to the administration of free DOX.

Conclusions

Exo-DOX-MEL appears to enhance the destructive effects of DOX in cancer cells, particularly those resistant to chemotherapy such as MDA-MB231 cells. It also plays a protective role in normal cells, which could be crucial in the treatment of drug resistance and the side effects caused by DOX.

Introduction

Despite recent advances in cancer treatment, DOX, as a class I anthracycline antibiotic, is still one of the main chemotherapy drug in the treatment of early and advanced breast cancer, which binds to DNA and inhibits its biosynthesis [1]. Chemotherapy with DOX is unfortunately associated with multidrug resistance (MDR) and its toxicity to healthy tissues, such as non-selective cardiac toxicity [2, 3]. Several studies have been conducted to find new strategies to maximize the clinical efficacy and limit the side effects of DOX. Therefore, there is an urgent need to identify compounds that can reduce the prescribed dose and their side effects, in addition to increasing the sensitivity of cancer cells to DOX. The use of carriers that can deliver the drug in a targeted manner to the target tissue may be more effective with reduced side effects [4, 5].

Despite recent advances in encapsulating drugs for cancer treatment and achieving effective drug accumulation in the tumor, there are still challenges in this field [6]. Most of the chemotherapy drugs have low solubility in water, as a result, it is necessary to use specialized carriers, such as liposomes, carbon nanotubes, gold nanoparticles, polymer nanoparticles and etc. Unfortunately, many of these drug carriers cause severe side effects, including organ toxicity or immune response, which can be due to the synthesis of these carriers from unnatural substances in the body. In addition, due to their premature destruction by the immune system, the circulation time of these carriers in the body decreases [7–9]. Therefore, biomimetic nanoparticles such as EXOs, which combine the unique properties of natural biological materials, such as cells or cell membranes, and the engineering versatility of synthetic nanoparticles, have been recently attracted considerable attention as effective drug delivery systems. Due to the fewer side effects, more studies have been conducted on EXOs than exogenous nanoparticles [10, 11]. EXOs are small extracellular vesicles (ECVs) with characteristics such as size 30 to 150 nm, lipid bilayer and endosomal origin, which are released by many cells into the extracellular space and recently, they have been considered as attractive carriers due to their low toxicity, biocompatibility, stability in circulation, and low immune response [12, 13]. EXOs have many roles that include cell-cell communication over long and short distances, as intercellular messengers, carriers of RNA, proteins, and small drugs [14].Since the source of EXO is important, mesenchymal stem cells (MSC) are recommended as an effective source of EXOs due to their stability, significant EXO production potential, and relatively high tolerance [15, 16].

Furthermore, given that a notable side effect of DOX involves the increase in free radical production, the integration of combination therapy with an adjuvant such as melatonin (MEL) can potentially overcome drug resistance, increase efficacy and reduce side effects by utilizing lower drug doses. It is suggested that MEL has potential antioxidant properties that can reduce DOX toxicity. In this study, an exosomal carrier derived from human adipose tissue stem cells was used to increase the effectiveness of DOX on cancer cells and reduce its side effects. Also, co-delivery of DOX with MEL in EXOs was performed to study its probable protective properties against the toxicity characteristics of DOX.

Material and method

Reagents:

Cell culture medium (Dulbecco's modified eagle medium, DMEM), fetal bovine serum (FBS), penicillin/streptomycin (P/S), trypsin–EDTA, and Phosphate buffered saline (PBS), Doxorubicin hydrochloride, Melatonin, Methylthiazolyldiphenyl-tetrazolium bromide (MTT), Dimethyl sulfoxide (DMSO), PKH26 (exosomes labeling) were purchased from Sigma-Aldrich (St. Louis, MO, USA). Collagenase Type II and trypan blue were purchased from Biochrom/Merck (Darmstadt, Germany). BCA protein assay kit was purchased from iNtRON Biotechnology Inc (Seoul, Rep. of Korea). The Annexin V-FITC apoptosis eBioscience detection kit was purchased from the Invitrogen company (USA).

Isolation of mesenchymal stem cells from human adipose tissue

Liposuction-derived fat (n = 4) was obtained from subcutaneous fat deposits on the abdominal wall of patients undergoing elective liposuction following the Coleman technique [17]. The study received approval from the local Ethical Committee on Human Studies (IR.MUBABOL.REC.1399.461), and all participants provided written informed consent to participate. The fat was mixed with cold phosphate-buffered saline (PBS) containing 1% Penicillin/Streptomycin (Pen/Strep) and transported to the laboratory in sterile containers, where it was processed within 1 h of liposuction. An average of 100 ml of adipose samples were washed several times with PBS, sliced, and digested in a 0.1% collagenase solution in a shaker incubator at 37°C and 80 rpm for 30–45 minutes [18, 19].

After inactivating the enzyme by adding complete culture medium (containing 20% FBS), the solution was centrifuged at 2000 rpm for 10 minutes to obtain the resulting cell suspension, which was then washed with PBS and filtered through a 40 µm cell strainer (BD Falcon, Durham, NC, USA). The resulting sediment was placed in RBC lysis solution (ammonium chloride 40%) for 10 minutes at room temperature. After a single washing and centrifugation step, the cells were seeded in culture flasks (Greiner Bio-One GmbH, Frickenhausen, Germany) containing DMEM/F12 with 20% FBS and 1% Pen/Strep. The cells were then incubated at 37°C in a humidified atmosphere with 5% CO2. After 24 h, the culture medium was changed, and this process was repeated every 48 h. Cell passaging was performed using 0.05% trypsin and 0.02% EDTA (Euroclone) once the cells reached 80–90% confluence.

Characterization of MSC isolated from adipose tissue

The cells were evaluated for MSC characteristics at the third passage. Cell morphology was assessed using a fluorescence microscope (Olympus microscope Bh2-RFCA, Japan), while stemness surface markers were analyzed using flow cytometry (BD Bioscience, San Jose, CA, USA). Expression of surface markers, including CD44 and CD90 (positive MSC markers), was assessed, along with CD34 and CD45 (negative MSC markers), in order to evaluate the stemness of the mesenchymal cells involved in the study [20].

After separating the cells from the flask by trypsin, they were washed by adding PBS solution and centrifuged at 1500 rpm for 5 minutes. Subsequently, each sample was supplemented with 5 µl of monoclonal antibodies and 5 µl of isotype control (Biolegend) in a final volume of 100 µl, using PBS, and the cells were incubated for 30 minutes at 4°C. Following incubation, excess antibodies were removed by

washing the samples with PBS. Finally, the samples were analyzed using the BD FACSCalibur machine (BD biosciences, San Jose).

Isolation of EXOs from the conditioned medium of MSC cells

MSCs in the fourth passage were cultured in T75 flasks with DMEM F12 culture medium containing 10% FBS and incubated at 37°C. To eliminate the interference of FBS materials, especially FBS-EXOs, an FBS-free medium was used. In order to minimize cell stress resulting from the absence of FBS, the amount of FBS was gradually decreased. The FBS concentration was sequentially reduced to 10%, 8%, 4%, 2%, 1%, and eventually 0%. After 24 h of exposure to FBS-free media (0%), culture medium or conditioned medium was collected [21, 22].

The EXOs extraction was performed by ultracentrifugation as a gold standard method (the Beckman Opti ma TLX Ultracentrifuge (CA, USA)) [23, 24]. Briefly, the conditioned medium was centrifuged at 200 g for 10 minutes, 2000 g for 10 minutes and 20000 g for 30 minutes to remove debris and other cellular bodies such as apoptotic bodies and larger EVs. Finally, the supernatant was collected and filtered with a 0.22 micrometer filter. The conditioned medium was ultracentrifuged at 120,000g for 120 minutes at 4°C, and the pelleted EXOs was washed in sterile PBS and filtered with a 0.22 µm filter to remove cellular materials and proteins. Again, the sample was ultracentrifuged for 90 minutes at 120,000g at 4°C. The resulting precipitate was resuspended in 200 µl of sterile PBS containing 1% Pen/Strep and stored at -80°C [25].

Exosome characterization

To confirm the extracted EXOs, we used TEM, DLS, western blot for the size and nature of EXOs, and also BCA kit for measuring the protein contents of EXOs.

Transmission electron microscopy

Transmission electron microscopy (TEM) (Philips CM30 electron microscope) was used for morphological evaluation of isolated EXOs. The EXOs were resuspended in PBS and fixed with 2% paraformaldehyde for 30 min at room temperature. Immobilized EXOs were placed on Formvar-carbon copper grids, which were treated with ultraviolet light, to reduce static electricity.

Dynamic Light Scattering Particle Size

The average size and size distribution of EXOs were evaluated using dynamic light scattering (DLS). DLS uses fluctuations in the intensity of scattered light to estimate the size of particles with a diameter of 1 nm to 6 µm. For this purpose, 20 µL of EXOs sample was diluted in PBS and their size was evaluated by DLS Zetasizer Nano ZS (Malvern Instruments, UK), and the results were analyzed using Zetasizer v7.11 software (Malvern Corp).

Immunoblotting

Western-blot method was used to identify EXOs markers such as CD9, CD81, CD63, and Calnexin. The cells were lysed by RIPA buffer (Tris-HCL, EDTA, NaCl, Sodium Deoxycholate, SDS, Protease inhibitor cocktail, Triton NP40 1%) and boiled at 95°C for 10 min with Laemmli sample buffer. Protein content was quantified using a standard Bradford assay. Resolved proteins in 10% SDS-PAGE were then transferred to nitrocellulose membranes, was placed in blocking solution (5% w/v skim milk powder in tris-buffered saline (TBS))-Tween buffer and incubated separately with CD9, CD81, CD63, and calnexin specific primary antibodies (cell guidance systems, UK) at the supplier's recommended dilutions overnight at 4°C. After subsequent washing, the membranes were further incubated with horseradish peroxidase coupled secondary antibodies (Abcam, Cambridge, UK). Bound Proteins were visualized using the ECL prime western blotting detection system (GE Healthcare, UK).

Measuring the protein content of EXOs using the BCA method

The concentration of exosomal proteins was quantified using the BCA method (SMART™ microBCA Protein Assay Kit, iNtRON Biotechnology Inc., Korea), following the manufacturer's instructions. In brief, 200 µl of the Working Solution (WS) was added to each well containing 10 µl of sample and standard, and then incubated at 37°C for 30 minutes. The absorbance was measured at 562 nm, and the calibration curve was calculated by plotting the absorbance against the concentration of the standards.

EXOs labeling and cell uptake assay

The EXOs were labeled with PKH26 (Sigma-Aldrich, St.Louis, MO, USA), a red-orange lipophilic dye, according to the manufacturer's instructions [26]. One hundred µg of EXOs (100 µl) and 4 µl PKH26 were separately diluted in 100 µL diluent C. The EXOs were mixed with PKH26 and incubated for 5 minutes at 37°C under darkness. The reaction was stopped by adding an equal volume of 1% BSA, and the mixture was ultracentrifuged at 120,000g for 90 min at 4°C to remove excess dyes. Mcf-7 cells (1×105 cells/well) were seeded in a 48-well plate, and 25 µg of labeled EXOs was added to each well. After 24 h, the cells were washed with PBS and fixed by 4% paraformaldehyde. The nuclei were stained by DAPI fluorescent (Sigma-Aldrich, USA), and examined using an inverted fluorescence microscope (Nikon TE300, Tokyo, Japan).

Preparation of the DOX and MEL-loaded EXOs, and Redetermination of EXOs properties

The sonication method, a preferred technique for loading drugs into EXOs [27], was used for transferring DOX and MEL to EXOs according to the method by Kim et al [7], with some modifications. Sonication was performed using a Sonoplus ultrasonic homogenizer HD2070 (BANDELIN) at 20% amplitude, with 6 cycles of 20 seconds on/off for three minutes and an 80-second cooling period between each cycle. After sonication, the EXO-DOX and EXO-MEL solutions were incubated at 37°C for 60 minutes to allow for recovery of the exosomal membrane. Excess free drug was separated from EXO-DOX and EXO-MEL by ultracentrifugation at 120,000 g for 90 minutes at 4°C.

The amount of drug loading in EXOs was determined by measuring the absorbance of each drug using a spectrophotometer. The quantity of free (unencapsulated) DOX and MEL in the supernatant was calculated using a UV-Vis spectrophotometer with a calibration curve of DOX and MEL at wavelengths of 480 nm and 285 nm, respectively. The encapsulation efficiency (EE) was calculated using the following formula [28]:

$$\mathbf{EE\%:}\ \frac{(\mathrm{Totaldrugadded})-(\mathrm{Freenonentrappeddrug})}{\mathrm{Totaldrugadded}}\times 100$$

After loading the drug in EXOs, TEM and DLS were used according to the above-mentioned protocol to reconfirm the integrity of the EXOs.

Release of DOX and MEL from EXOs

DOX release from EXOs was determined according to the following method. DOX and MEL-loaded EXOs were immersed in dialysis tubes and dispersed in 5 mL of PBS with different pH values including 5.3 for cancer cells and 7.4 for normal cells under sink conditions. The concentration of DOX and MEL at 37°C and at time intervals of 0, 1, 3, 6, 12, 24, 36 h was calculated according to the DOX and MEL calibration curve of the UV-Vis spectrophotometer at 480 and 285 nm with the following formula [29]:

$$\text{Drug Release (\%)} = \frac{\mathrm{AmountofDrugRelease}}{\mathrm{AmountofDrugonExosomes}}\times 100$$

Cellular uptake assay of DOX and Exo-DOX

The quantitative and qualitative cellular uptake of DOX and EXO-DOX in cancer and normal cells was investigated using fluorescence microscopy and flow cytometry analysis, which relied on the intrinsic fluorescence emission of DOX. For the flow cytometry analysis, cells were cultured in 6-well plates (5×105 per well) and incubated for 24 h. Subsequently, the cells were treated with DOX (positive control) and EXO-DOX. After 2 h, the cells were trypsinized, collected, and washed twice with cold PBS. The resulting precipitate was re-dissolved in cold PBS, and the DOX fluorescence intensity was evaluated using a FACScalibur flow cytometer (Becton Dickinson Immunocytometric Systems, San Jose, CA, USA) in the FL2 channel.

The cells were treated with DOX and EXO-DOX 24 h after cell culture, and the treatment lasted for 2 h. Subsequently, the cells were trypsinized and collected. After centrifugation, the cells were washed twice with cold PBS, and the resulting precipitate was placed on a slide for examination of the fluorescence intensity of DOX using a fluorescence microscope (Olympus Bh2-RFCA microscope, Japan).

The Cell treatment and cytotoxicity assay

We utilized MCF-7, MCF-10A, MDA-MB-231, and A-MSC cell lines to study the effect of EXOs-loaded drugs on breast cancer. To investigate the breast cancer model, MCF-7 (estrogen receptor-positive) cells were used as tumors affected by estrogen hormone and MDA-MB-231 (estrogen receptor-negative), which are aggressive and invasive triple-negative breast cancer (TNBC) cells that are resistant to several anticancer

agents. Additionally, the normal breast epithelial cells MCF-10a and A-MSC were included in the study to compare the treatment effects [30].

The MTT assay was conducted to examine the cytotoxic effects of Exo-loaded drugs on MCF-7, MCF-10A, MDA-MB-231, and A-MSC cells and to determine the IC50. Firstly, the cells were seeded in a 96-well plate. When the cells reached 80–90% confluency, the medium was removed and cells were washed with PBS. The fresh medium containing various concentrations of free-DOX, free-MEL, DOX/MEL, free-Exo, Exo-DOX, Exo-MEL, and Exo-DOX-MEL was added and incubated for 24, 48, and 72 h. Then, the supernatant was discarded and the cells were washed with PBS to remove the residual drug. 100 µL of 0.5 mg/mL MTT was added and further incubated for 4 h. Finally, supernatant liquid was removed and replaced with 150 µL of DMSO to dissolve the formazan crystals. The microplate was shaken on a shaker at 37°C for 10 min. The viability of the cells was determined by measuring the absorbance of each well at 570 nm by a multi-functional microplate reader with a reference wavelength of 630 nm. The cell viability was determined by comparing the mean absorbance of treated cells to untreated cells [31].

Cell Viability (%) = $\frac{\mathrm{A(Treatment)}}{\mathrm{A(Control)}}$ × 100 (where, A=absorbance)

Gene expression assay by Real Time PCR

After 24 h of treatment of cells with the IC50 concentration of the drug, total RNA was extracted using an RNA extraction kit (Favorgen, Taiwan) following the instructions provided by the manufacturer. Isolated RNAs were dissolved in 20 µL of diethylenepyrocarbonate-treated water (DEPC-treated water) (SinaClon. Iran) and the quantity and quality of RNA were determined using a spectrophotometer (NanoDrop Technologies, USA) and agarose gel electrophoresis, respectively. Total RNA was reverse transcribed according to the manufacturer's instructions using a cDNA synthesis kit (Yekta Tajhiz Azma Co, Iran).

After reverse transcription, the produced cDNA was used to Real-time PCR by SYBR Green PCR Master Mix (Ampliqon, Denmark) to analyze the P53, NANOG, and miR-34a expression status. The expression of the target genes was studied in comparison to the housekeeping gene using the comparative threshold cycle (Ct) approach. The data was derived via ΔCt calculations, where ΔCt = Ct (Target)-Ct (Reference). The $2^{-\Delta\Delta Ct}$ formula was used to calculate fold changes.

Analysis of apoptosis by flow cytometry and acridine orange/ethidium bromide stain

Annexin V and PI staining were used to evaluate the amount of apoptosis in groups receiving free-DOX, free-MEL, DOX/MEL, free-Exo, Exo-DOX, Exo-MEL, and Exo-DOX-MEL. The group that did not receive any treatment was considered as the control group. Annexin V and PI staining were used to evaluate the amount of apoptosis in the treated groups. The group that did not receive any treatment was considered as the control group.

The cell lines were cultured in six-well plates with a concentration of 2×10^5 cells in each well for 24 h. Subsequently, the cells were treated with free-DOX, free-MEL, DOX/MEL, free-Exo, Exo-DOX, Exo-MEL, and

Exo-DOX-MEL at their respective IC50 concentrations for 24 h. The cells were then trypsinized, collected, washed with PBS, and suspended in annexin binding buffer. The cell suspension was combined with 5µl of propidium iodide (PI) and 5µl of FITC Annexin V. After incubating for 15 minutes, 200 µl of binding buffer was added to each sample. Finally, a FACSCalibur flow cytometer was utilized to identify apoptotic cells.

Acridine orange/ethidium bromide (AO/EB) dye was used to qualitatively assess apoptosis. Twenty-four hours after cell treatment, 2.5 ×105 cells were harvested, washed with cold PBS and centrifuged. The precipitate was dissolved in 2 µl of staining solution containing 100 µg/ml acridine orange (AO) and 100 µg/ml ethidium bromide (EB). Also, 10µl of the suspension were transferred to glass slides and covered with a coverslip. The morphology of the cells was examined using a fluorescent microscope (Olympus Bh2-RFCA microscope, Japan) at wavelength 470/40 nm.

Statistical analysis

Results were presented as mean ± SD from at least 3 independent experiments. Statistical analysis was performed via GraphPad Prism 6 software (GraphPad Software, Inc., La Jolla, CA). One-way analysis of variance (ANOVA) was performed to determine the significance differences between study groups. Significant differences are shown as *$p < 0.05$, **$p < 0.01$, ***$p < 0.001$ and ****$p < 0.0001$.

Results and discussion

DOX is a widely used chemotherapy drug for treating breast cancer, but its clinical application is restricted by severe side effects and drug resistance. In our study, we encapsulated the chemotherapy drug DOX in the safe carrier exosomes (Exo), derived from mesenchymal stem cells obtained from human adipose tissue. Additionally, we included melatonin as an antioxidant in the above composition, with the aim of potentially achieving improved results.

The properties of MSCs were observed from cells isolated from adipose tissue.

Examination of adipose tissue-derived MSCs at passage 3 revealed a fibroblast morphology throughout the culture when observed under an inverted microscope (Fig. 1). Characteristic surface markers on MSCs were identified using flow cytometry. The expression of negative markers, CD45 and CD34, was found to be 1.37% and 2.19%, respectively, while the expression of positive markers, CD44 and CD90, was 99.8% and 99.5%, respectively (Fig. 2). These results, along with the morphology of the cells, confirm that these cells exhibit typical characteristics of stem cells, aligning with findings from similar studies [32, 33].

The particles extracted from MSCs confirmed the characteristics of EXOs.

EXOs were successfully isolated from AMSC-conditioned media by ultracentrifuge method. TEM observations of the EXOs revealed a typical spherical and oval shape for AMSC- EXOs (Fig. 3-A). Additionally, dynamic light scattering (DLS) characterization indicated an average size of 101.7 nm with a peak at 80.72 nm for these EXOs. (Fig. 3-B). Moreover, western blot analysis of surface markers suggested

that EXOs were rich in tetraspanins as positive markers such as CD9, CD63 and CD81, while Calnexin was not expressed as a negative marker in EXOs. (Fig. 3-C). These results are consistent with the other results in confirming the characteristics of EXOs in terms of shape, size and expression of surface proteins [34, 35].

Protein content of Exos was measured using BCA method. BCA is a standard method to determine the concentration of Exos. After lysing the Exos, the protein concentration was measured. The results indicated the protein concentration of the Exos, which served as the basis for determining the amount of Exos used in the subsequent stages of the study.

EXOs have the capability to be uptake up by cells.

To investigate whether Exos extracted from MSCs are able to bind and enter cancer cells, cancer cells were treated with EXOs whom previously labeled with PKH26 dye. PKH26 as a dye bound to the Exos was observed inside the cell by using a fluorescent microscope; the cellular absorption of the Exos was confirmed. Red and blue colors represent PKH26 and DAPI, respectively (Fig. 4).

Drug entrapment and release rate from Exos and revisited Exos structure

DOX as an anti-cancer drug and Mel as an antioxidant were loaded in Exos and the loading and release capacity of these drugs from Exos was evaluated. Among the drug loading methods evaluated, sonication demonstrated the highest potential for facilitating drug entry into Exos [36]. The quantity of encapsulated DOX was determined using a spectrophotometric method, measuring the autofluorescent characteristics of DOX at 480 nm, while the amount of encapsulated Mel was measured at 285 nm against serial dilutions of known standards. Our results revealed that approximately 37% of DOX and 32% of Mel were successfully loaded into Exos [37].

The drug loading in Exos is influenced by several factors including the loading method, the source of Exos, and the size and solubility of the drug. Various studies have reported different loading and encapsulation percentages of drugs in EXOs [38, 39], while the results of Chunyan Yang et al. were almost similar to our work [40]. TEM and DLS were utilized to assess whether sonication or drug transfer had any impact on the structure of EXOs. TEM images showed that the morphology of Exos remained almost unchanged after drug loading. Also, DLS showed no significant change in the size of EXOs (Fig. 5). The results indicate no change in the nature of the EXOs for drug storage and release, and these results were confirmed by others [38].

DOX is affected by pH due to having amine groups as functional groups. Therefore, the release capacity was investigated at different pH of 5 (environment of cancer cells) and 7.4 (conditions of normal cells). The release rate of DOX and EXO-DOX at pH: 5 were 66.7% and 90.5% after 36 h, respectively, but the release profiles of DOX and EXO-DOX after 36 h at pH: 7.4 were 35.4% and 28.6%, respectively. Also, the

release rate of Mel and EXO-MEL at pH: 5 were 25.2% and 33.6%, after 36 h, but the release profiles of Mel and EXO-MEL were 32.3% and 42.4% after 36 h at pH 7.4, respectively.

These results clearly demonstrate that the pH of the medium has a significant impact on the release rate of DOX and MEL [41]. Under conditions mimicking those of cancer cells (pH 5), DOX and MEL loaded in EXOs are released more rapidly than free DOX and MEL, indicating an increase in cytotoxicity under acidic conditions. Consequently, there is improved effectiveness and targeting of drug accumulation in cancerous conditions.

Conversely, under conditions mimicking normal cells (pH 7.4), EXO-DOX is released at a slower rate than free DOX, while EXO-MEL is released at a faster rate than free MEL. This discrepancy leads to decreased toxicity in normal cells (reducing side effects of DOX) and an increased presence of antioxidants (MEL) (Fig. 6). Consistent with our findings, other studies have reported similar results, with authors concluding that acidic environments in endosomes and lysosomes can induce drug release [42–44].

Qualitative and quantitative intracellular uptake of Exo-DOX

As illustrated in Fig. 7, both DOX-loaded Exos and free DOX were efficiently absorbed and internalized by both cancer and normal cells within 4 h. The uptake process appeared to be completed within this time frame, as indicated by the high fluorescence intensity observed in the cells. Flow cytometry analysis corroborated these observations, demonstrating that in MCF-7 and MDA-MB231 cells, 76.4% and 45.3% of free DOX, and 96% and 82.1% of EXO-DOX, were absorbed after 4 h, respectively. These findings suggest that Exo-DOX exhibits greater absorption compared to free DOX within the same time period, thus heightening the impact of DOX on these cells. In MCF-10A and A-MSC cells, the absorption rates after 4 h were 80.9% and 74.1% for free DOX, and 65.7% and 69% for EXO-DOX, respectively. These outcomes validate the diminished absorption of EXO-DOX in comparison to free DOX, leading to reduced accumulation in normal cells. Consequently, the initially low absorption of free DOX in cancer cells is largely compensated by the presence of EXO, magnifying the impact of DOX on these cells. However, in normal cells, EXO diminishes DOX absorption, consequently lowering cell death and its associated effects.

In vitro anticancer effect of functional EXOs-mediated co-delivery of DOX and MEL

In order to assess the potential enhancement of the anticancer effect through the combined delivery of DOX and MEL with EXOs, we evaluated the viability of breast cancer cells, normal cells, and stem cells treated with free-DOX, free-MEL, DOX/MEL, free-Exo, Exo-DOX, Exo-MEL, and Exo-DOX-MEL over the course of 24, 48, and 72 h.

As shown in the Fig. 8, the cytotoxicity assay of different treatment showed dose- and time-dependent manner inhibition of cell proliferation. In MCF-7 cells, DOX/MEL, Exo-DOX and Exo-MEL caused greater toxicity than free-DOX and MEL in their free form. However, the most striking difference was observed with Exo-MEL compared to the free form of MEL and Exo. On the other hand, free-Exo exhibited slightly greater

effectiveness than free-MEL and achieved a 50% inhibitory concentration within 72 h. Moreover, the combination of Exo-DOX-MEL showed a significantly superior effect on cell death compared to other compounds. In MCF-10A and AMSC cells, MEL and Exo were able to reverse the effect of DOX to a large extent, and free-DOX showed the lowest IC_{50}.

In MDA-MB231 cells, free-DOX could kill 50% of the cells at a concentration of 5.4 µg/ml. However, the combination of DOX with MEL or the loading of DOX in Exos did not exhibit a significant effect on enhancing the efficacy of DOX in causing cell death in this particular cell line. But, when the co-delivery of DOX and MEL took place within Exo, it demonstrated the most pronounced effect in inducing cell death in MDA-MB231 cells.

In general, Exo increases DOX toxicity in MCF-7 and MDA-MB231 cells and decreases it in MCF-10A and AMSC cells. As a result, by targeting cancer cells, it can prevent unwanted side effects on normal cells to some extent. The selectivity index (SI) was calculated as the ratio of cytotoxicity (IC50) observed in normal cells (MCF-10a and AMSC) to that in cancer cells (MCF-7 and MDA-MB-231). An SI value greater than 3 suggests the selectivity of the cytotoxic effect of DOX specifically toward MCF-7 and MDA-MB-231 cells [30].

According to the results of Tables 2 and 3, free DOX cannot act selectively on any of MCF-7 and MDA-MB231 cell lines. Although the combination of DOX with MEL was able to reduce the IC50 compared to free DOX, it was selective only in MCF-7 cells over A-MSC cells. Furthermore, the outcomes from the encapsulation of DOX in EXOs were similar to the results of combining DOX with MEL. Co-delivery of DOX and MEL in EXOs (Exo-Dox-Mel) amplified the selectivity index in MCF-7 and MDA-MB-231 cells. Subsequently, it can be concluded that, in contrast to free DOX, unlike free DOX, which affects not only cancer cells but also rapidly dividing normal cells, the Exo-DOX-Mel demonstrates selectivity toward breast cancer cells while exhibiting less impact on normal cells.

Table 1
IC50 concentration of free-DOX, free-MEL, DOX/MEL, free-Exo, Exo-DOX, Exo-MEL, and Exo-DOX-MEL against Saos-2, MG63, and hBM-MSC for 24, 48, and 72 h.

IC_{50}		free-DOX (µg/mL)	free-MEL (µg/mL)	DOX/MEL (µg/mL)	free-Exo (µg/mL)	Exo-DOX (µg/mL)	Exo-MEL (µg/mL)	Exo-DOX-MEL (µg/mL)
MCF-7	24h	2.21	-	2.08	50	1.83	5.65	0.89
	48h	1.93	-	1.49	37.5	0.98	5.07	0.71
	72h	1.2	33.54	0.86	18.75	0.91	3.64	0.38
MCF-10A	24h	2.11	-	4.04	-	4.6	-	5.35
	48h	1.06	-	1.1	-	1.25	-	2.49
	72h	0.64	-	0.71	-	0.76	34.86	1.79
MDA-MB231	24h	5.4	-	4.68	-	3.48	12.22	1.76
	48h	2.88	-	3.13	-	2.86	8.09	0.81
	72h	1.67	-	3.08	39.49	1.47	6.17	0.57
A-MSC	24h	4.8	-	5.65	-	6.49	-	8.52
	48h	3.95	-	6.34	-	6.41	-	9.15
	72h	3.06	-	4.14	-	5.73	-	10.07

Table 2
Selectivity index (SI) of treatments for MCF-7 and MDA-MB231 cells.

SI		free-DOX (µg/mL)	free-MEL (µg/mL)	DOX/MEL (µg/mL)	free-Exo (µg/mL)	Exo-DOX (µg/mL)	Exo-MEL (µg/mL)	Exo-DOX-MEL (µg/mL)
MCF-10A/MCF-7	24h	0.95	-	1.9	-	2.51	-	6.01
	48h	0.54	-	0.73	-	1.27	-	3.50
	72h	0.53	-	0.82	-	0.83	9.57	4.71
A-MSC /MCF-7	24h	2.17	-	2.71	-	3.54	-	9.57
	48h	2.04	-	4.25	-	6.54	-	12.88
	72h	2.55	-	4.81	-	6.29	-	26.5
MCF-10A/MDA-MB231	24h	0.39	-	0.86	-	1.32	-	3.03
	48h	0.36	-	0.35	-	0.43	-	3.07
	72h	0.38	-	0.23	-	0.51	5.6	3.14
A-MSC/MDA-MB231	24h	0.88	-	1.20	-	1.86	-	4.84
	48h	1.37	-	2.02	-	2.24	-	11.29
	72h	1.83	-	1.34	-	3.89	-	3.14

Gene expression changes as a result of the combination of MEL with DOX and loading in EXO

Since DOX interacts with double-stranded DNA and increases free radicals, it causes double-stranded breaks in DNA structure, DNA damage and induction of apoptosis [45]. Therefore, we analyzed the mechanistic effects of DOX in combination with MEL loading in EXOs at the gene level by assessing the expression of p53, NANOG, and MIR-34a genes in MCF-7, MCF-10A, MDA-MB231, and A-MSC cell lines. P53 is recognized as the principal regulator of the cell cycle and apoptosis [46].

Two main comparisons were conducted: one toward untreated cells (control) and the other toward cells that received only DOX (free DOX), aimed at more precisely elucidating the mechanism of the drug's impact when using the EXO carrier and MEL antioxidant. In the current research, we demonstrated that the p53 gene, recognized as the primary regulator of the cell cycle and apoptosis, exhibited increased expression in cells treated with DOX, aligning with our expectations. In the presence of free DOX, MCF-10A and MDA-MB231 cells recorded the highest and lowest p53 gene expression, respectively, which indicates the inability of free DOX to effectively destroy resistant breast cancer cells (MDA-MB231) and side effects on the cells. In addition, free DOX caused a significant increase in p53 gene expression in normal breast tissue cells (MCF-10A) and mesenchymal stem cells (MSCs) compared to the control group, which indicates the beginning of apoptosis. EXO-loaded DOX showed a significant increase in p53 gene

expression compared to free DOX in MCF-7, but had a protective role in MCF-10A and MSC cells, which caused the reduction of apoptosis due to the reduction of p53 gene expression. But in MDA-MB231 cells, EXO-DOX did not cause much change compared to free DOX. Co-delivery of DOX with MEL in EXOs significantly increases the expression of p53 gene in cancer cells and has a much greater protective effect in normal cells compared to the control group and the group receiving free DOX (Fig. 9).

p53 is directly related to NANOG; a key transcription factor for the maintenance of embryonic stem cell pluripotency, which has recently been shown to be overexpressed in many types of human cancers, including breast cancer and it is related to increasing drug resistance properties of cancer cells. NANOG expression is modulated through p53 deacetylation, and induction of p53 expression by DNA damage represses NANOG and induces embryonic stem cells (ESC) to differentiate into cell types that can undergo cell death to efficiently remove damaged DNA, which ultimately prevents tumorigenesis [47, 48].

Our findings indicate that the expression of NANOG significantly decreased in MCF-7, MCF-10A, and A-MSC cells treated with free DOX, in comparison to the control group. This reduction in NANOG expression has the potential to induce P53-mediated cell death [49]. In the case of MDA-MB231 cells, the effect of free DOX on NANOG expression was observed to exhibit a slight decrease compared to the control group, which was not statistically significant and indicated a possible connection with the inherent resistance of these cells to chemotherapy agents. In both the DOX-MEL and EXO-DOX groups, the expression of NANOG was significantly downregulated in MDA-MB231 and MCF-7 cells, in comparison to the free DOX group. Conversely, an elevated expression of NANOG was observed in MCF-10A and A-MSC cells when compared to the free DOX group. In the DOX-MEL, EXO-DOX, and EXO-DOX-MEL treatment groups, a notable decrease in the expression of NANOG was observed in MDA-MB231 and MCF-7 cells when compared to the free DOX group. Conversely, increased NANOG expression was detected in MCF-10A and A-MSC cells when compared to the free DOX group. Of particular significance, the EXO-DOX-MEL group exhibited the most pronounced changes, highlighting its effectiveness in comparison to the other treatment groups.

These results demonstrate that the loading of DOX in EXOs in combination with MEL (EXO-DOX-MEL) leads to a reduction in NANOG expression in cancer cells, thereby amplifying the toxicity of DOX in these cell lines and inducing heightened apoptosis through P53 activation. Moreover, increasing Nanog expression in normal cells may partially reduce the DOX cytotoxic effects and prevent the destruction of these cells [50].

In this regard, Ebeid et al showed that free DOX combined with berberine can significantly reduce the expression of NANOG compared to the control group [49]. Also, similar studies emphasized that inhibiting Nanog, reverses resistance to chemotherapy and radiation therapy [51]. It was also found that removing NANOG by reducing the expression of MDR1 increases the chemical sensitivity of liver cancer cells to DOX [52].

Cardiotoxicity is a known side effect of DOX and has been linked to the activity of MiR-34a. MiR-34a plays a crucial role in the p53-mediated antitumor process, and its upregulation in tumor cells can enhance their sensitivity to chemotherapy drugs [47, 53]. Moreover, research findings indicate that miR-34a acts as a

barrier to reprogramming by suppressing pluripotency marker genes, including NANOG. The repression of Nanog by p53 occurs through direct transcriptional silencing as well as indirect post-transcriptional silencing mediated by miR-34 [54, 55].

By assessing the levels of MiR-34a, our study approved the findings of p53. Following DNA damage, the activation of miR-34a by p53 arrested the cell cycle and enhanced apoptosis in breast cancer cells upon treatment with EXO-DOX-MEL. Conversely, in normal cells, miR-34a played a protective role, potentially guarding against DOX-induced cardiotoxicity.

In the study of Lee et al., miR-34a by inhibiting Sirt1 expression leads to increased activity of p53, suppression of cell reprogramming by Nanog and finally apoptosis [47]. In this regard, Zheng et al. stated that the overexpression of MiR-34a enhances the inhibitory effect of DOX on HepG2 cancer cells [55]. In addition, Correia Marques et al published that high expression of miR-34a improves the response to DOX in diffuse B-cell lymphoma [56]. In addition, Deng et al found that miRNA-34a can enhance the antitumor activity of DOX in the treatment of triple negative breast cancer [57].

The co-delivery of DOX and MEL within EXOs enhances the rate of apoptosis.

The apoptosis rate was evaluated using Annexin V and PI staining. MCF-7, MCF-10A, MDA-MB231, and A-MSC lines were treated with free-DOX, free-MEL, DOX/MEL, free-Exo, Exo-DOX, Exo-MEL, and Exo-DOX-MEL. The control group consisted of untreated cells (Fig. 10).

Treatment with free DOX in four cell lines include MCF-7, MCF-10A, MDA-MB231, and A-MSC caused 47.9%, 52.5%, 18.19%, and 46.1% apoptosis (sum of late and early apoptosis), respectively. Among the cell lines tested, the highest and lowest cell death was occurred in MCF-10A and MDA-MB231 cell lines, respectively, indicating the toxicity of DOX on normal cells and the relative resistance of triple negative cancer cells. Interestingly, the combination of MEL with DOX not only increased the death rate in MCF-7 cells (66.4%) but also enhanced toxicity in normal cells (MCF-10A: 38.2% and A-MS: 39.5%). In contrast, its impact on MDA-MB231 cells was relatively modest (23.05%).

In our study, Exo, primarily utilized as a drug carrier, exhibited a notable self-healing effect. It demonstrated significant apoptotic effects of Exos in MCF-7, MCF-10A, MDA-MB231, and A-MSC cells, resulting in respective cell death rates of 37.68%, 8.05%, 13.58%, and 6.59%. These findings suggest a higher susceptibility of cancer cells to Exo-induced cell death compared to normal cells. Exo in combination with DOX or MEL could slightly enhance the effects of these drugs alone. But the highest rate of cancer cell death was 80.82% and 56.1% apoptosis in MCF-7 and MDA-MB231, respectively, in treatment with Exo-DOX-MEL. Also, treatment with Exo-DOX-MEL in normal cells resulted in 18.13% and 7.14% apoptosis in MCF-10A and A-MSC, respectively. Subsequently, co-delivery of DOX and MEL in Exo could increase the toxicity in cancer cells, especially MDA-MB231 cells, which were resistant to free DOX. It also greatly protected normal cells from damage caused by DOX. This function can be partially attributed to melatonin, which plays a role as an antioxidant in destroying cancer cells and protecting normal cells [58].

Figure 11 shows the images of apoptosis evaluation and apoptotic cells using AO/EB staining. Live cells are uniformly green in color. Early apoptotic cells have a yellow color, chromatin density and membrane bubbles, while late apoptotic cells have orange to red pieces, fragmentation of chromatin and nucleus, and the presence of apoptotic bodies. Our results showed the toxicity of free DOX on MCF-7, MCF-10A, and A-MSC cells without significant effect on MDA-MB231 cells. Treatment with DOX/MEL, Exo-DOX and Exo-DOX-MEL enhances the effect of DOX in cancer cells and protects normal cells from DOX toxicity, among them, the most effective combination is Exo-DOX-MEL, which has shown a significant effect even on MDA-MB231 cells.

Conclusion

This study focuses on the encapsulation of two therapeutic agents, DOX (a chemotherapy drug) and MEL (an antioxidant), within EXOs derived from human adipose tissue mesenchymal stem cells. The combination of DOX and MEL exhibits several advantages. Firstly, it demonstrates pH-responsive release behavior, allowing for precise drug delivery. Additionally, it showcases a high loading capacity, enabling efficient incorporation of both agents. Notably, this combination demonstrates enhanced toxicity towards breast cancer cells, particularly those resistant to treatment, while minimizing adverse effects on normal cells. Furthermore, the presence of MEL not only enhances the toxic effect of DOX, but also mitigates its side effects on normal cells. Consequently, Exo-DOX-MEL formulation effectively reduces the required dosage of DOX as indicated by a reduction in IC50 values. Overall, our findings highlight the potential of Exo-DOX-MEL as a probable promising therapeutic strategy that maximizes the efficacy of DOX while minimizing its toxicity towards normal cells.

Abbreviations

MSC: Mesenchymal stem cells

A-MSC: Adipose tissue mesenchymal stem cells

EXO: Exosome

EV: Extracellular vesicles

DOX: Doxorubicin

MEL: Melatonin

Declarations

Author statement

Moein Shirzad, Hadi Parsian. designed the study and drafted the initial manuscript. **Abdolreza Daraei**. analyzed the data and performed statistical analyses. **Hossein Najafzadehvarzi, Nazila Farnoush.** contributed to the critical revision of the manuscript . All authors reviewed the drafted manuscript for critical content and approved the final version. The corresponding author attests that all listed authors meet authorship criteria and that no others meeting the criteria have been omitted.

Ethics approval and consent to participate

The study protocols were approved by the Ethics Committee of Babol University of Medical Sciences (Thesis no: 9911423 and ethical code: IR.MUBABOL.REC.1399.461).

Consent for publication

Not applicable.

Competing interests

The authors declare that they have no competing interests.

Acknowledgments

This research was financially supported by Babol University of Medical Sciences. (Thesis no: 9911423 and ethical code: IR.MUBABOL.REC.1399.461).

Funding

The research protocol was approved and supported by Babol University of Medical Sciences.

References

1. Bhatnagar, S., et al., *Dissolvable microneedle patch containing doxorubicin and docetaxel is effective in 4T1 xenografted breast cancer mouse model.* International Journal of Pharmaceutics, 2019. **556**: p. 263-275.
2. Pugazhendhi, A., et al., *Toxicity of Doxorubicin (Dox) to different experimental organ systems.* Life sciences, 2018. **200**: p. 26-30.
3. Al-Malky, H.S., et al., *Modulation of doxorubicin-induced expression of the multidrug resistance gene in breast cancer cells by diltiazem and protection against cardiotoxicity in experimental animals.* Cancer Cell International, 2019. **19**(1): p. 1-10.
4. Ashrafizadeh, M., et al., *Polychemotherapy with curcumin and doxorubicin via biological nanoplatforms: enhancing antitumor activity.* Pharmaceutics, 2020. **12**(11): p. 1084.
5. Hadla, M., et al., *Exosomes increase the therapeutic index of doxorubicin in breast and ovarian cancer mouse models.* Nanomedicine, 2016. **11**(18): p. 2431-2441.

6. Gharpure, K.M., et al., *Nanotechnology: future of oncotherapy.* Clinical Cancer Research, 2015. **21**(14): p. 3121-3130.
7. Kim, M.S., et al., *Development of exosome-encapsulated paclitaxel to overcome MDR in cancer cells.* Nanomedicine: Nanotechnology, Biology and Medicine, 2016. **12**(3): p. 655-664.
8. Mitragotri, S., P.A. Burke, and R. Langer, *Overcoming the challenges in administering biopharmaceuticals: formulation and delivery strategies.* Nature reviews Drug discovery, 2014. **13**(9): p. 655-672.
9. Vargason, A.M., A.C. Anselmo, and S. Mitragotri, *The evolution of commercial drug delivery technologies.* Nature biomedical engineering, 2021. **5**(9): p. 951-967.
10. Tan, S., et al., *Cell or cell membrane-based drug delivery systems.* Theranostics, 2015. **5**(8): p. 863.
11. Batrakova, E.V. and M.S. Kim, *Using exosomes, naturally-equipped nanocarriers, for drug delivery.* Journal of Controlled Release, 2015. **219**: p. 396-405.
12. Li, X., et al., *Challenges and opportunities in exosome research—Perspectives from biology, engineering, and cancer therapy.* APL bioengineering, 2019. **3**(1).
13. Ramesh, D., et al., *Extracellular vesicles as novel drug delivery systems to target cancer and other diseases: Recent advancements and future perspectives.* F1000Research, 2023. **12**(329): p. 329.
14. Sun, Y., et al., *Mesenchymal stem cells-derived exosomes for drug delivery.* Stem cell research & therapy, 2021. **12**: p. 1-15.
15. Oveili, E., et al., *The potential use of mesenchymal stem cells-derived exosomes as microRNAs delivery systems in different diseases.* Cell Communication and Signaling, 2023. **21**(1): p. 1-26.
16. Rao, D., et al., *Advances in mesenchymal stem cell-derived exosomes as drug delivery vehicles.* Frontiers in bioengineering and biotechnology, 2022. **9**: p. 797359.
17. Coleman, S.R., *Structural fat grafting.* Aesthetic Surgery Journal, 1998. **18**(5): p. 386-388.
18. Chang, H., et al., *Safety of adipose-derived stem cells and collagenase in fat tissue preparation.* Aesthetic plastic surgery, 2013. **37**: p. 802-808.
19. Zhou, J., et al., *Adipose derived mesenchymal stem cells alleviated osteoarthritis and chondrocyte apoptosis through autophagy inducing.* Journal of cellular biochemistry, 2019. **120**(2): p. 2198-2212.
20. Camilleri, E.T., et al., *Identification and validation of multiple cell surface markers of clinical-grade adipose-derived mesenchymal stromal cells as novel release criteria for good manufacturing practice-compliant production.* Stem cell research & therapy, 2016. **7**(1): p. 1-16.
21. Ding, H., et al., *Extracellular vesicles and exosomes generated from cystic renal epithelial cells promote cyst growth in autosomal dominant polycystic kidney disease.* Nature communications, 2021. **12**(1): p. 4548.
22. Lehrich, B.M., Y. Liang, and M.S. Fiandaca, *Foetal bovine serum influence on in vitro extracellular vesicle analyses.* Journal of Extracellular Vesicles, 2021. **10**(3).
23. Tsiapalis, D. and L. O'Driscoll, *Mesenchymal stem cell derived extracellular vesicles for tissue engineering and regenerative medicine applications.* Cells, 2020. **9**(4): p. 991.

24. Tiwari, S., et al., *Preparation and characterization of extracellular vesicles.* American Journal of Reproductive Immunology, 2021. **85**(2): p. e13367.
25. Mobahat, M., et al., *Curcumin-loaded human endometrial stem cells derived exosomes as an effective carrier to suppress alpha-synuclein aggregates in 6OHDA-induced Parkinson's disease mouse model.* Cell and Tissue Banking, 2023. **24**(1): p. 75-91.
26. Dominkuš, P.P., et al., *PKH26 labeling of extracellular vesicles: Characterization and cellular internalization of contaminating PKH26 nanoparticles.* Biochimica et Biophysica Acta (BBA)-Biomembranes, 2018. **1860**(6): p. 1350-1361.
27. Raghav, A. and G.-B. Jeong, *A systematic review on the modifications of extracellular vesicles: a revolutionized tool of nano-biotechnology.* Journal of Nanobiotechnology, 2021. **19**(1): p. 1-19.
28. Tran, P.H., et al., *Development of a nanoamorphous exosomal delivery system as an effective biological platform for improved encapsulation of hydrophobic drugs.* International journal of pharmaceutics, 2019. **566**: p. 697-707.
29. Munagala, R., et al., *Bovine milk-derived exosomes for drug delivery.* Cancer letters, 2016. **371**(1): p. 48-61.
30. Razak, N.A., et al., *Cytotoxicity of eupatorin in MCF-7 and MDA-MB-231 human breast cancer cells via cell cycle arrest, anti-angiogenesis and induction of apoptosis.* Scientific reports, 2019. **9**(1): p. 1514.
31. Gong, C., et al., *Functional exosome-mediated co-delivery of doxorubicin and hydrophobically modified microRNA 159 for triple-negative breast cancer therapy.* Journal of nanobiotechnology, 2019. **17**(1): p. 1-18.
32. Bourin, P., et al., *Stromal cells from the adipose tissue-derived stromal vascular fraction and culture expanded adipose tissue-derived stromal/stem cells: a joint statement of the International Federation for Adipose Therapeutics and Science (IFATS) and the International Society for Cellular Therapy (ISCT).* Cytotherapy, 2013. **15**(6): p. 641-648.
33. Mendicino, M., et al., *MSC-based product characterization for clinical trials: an FDA perspective.* Cell stem cell, 2014. **14**(2): p. 141-145.
34. Li, C., et al., *Colorimetric aptasensor based on spherical nucleic acid-induced hybridization chain reaction for sensitive detection of exosomes.* Talanta, 2023. **258**: p. 124453.
35. Sarte, L., et al., *Tumour-derived exosomes contribute to a pro-tumourigenic inflammatory microenvironment in cancer.* Journal of Extracellular Vesicles, 2018. **7**: p. 48-48.
36. Lee, J., et al., *Exosome-based drug delivery systems and their therapeutic applications.* RSC advances, 2022. **12**(29): p. 18475-18492.
37. Bagheri, E., et al., *Targeted doxorubicin-loaded mesenchymal stem cells-derived exosomes as a versatile platform for fighting against colorectal cancer.* Life Sciences, 2020. **261**: p. 118369.
38. Wang, J., et al., *Inflammatory tumor microenvironment responsive neutrophil exosomes-based drug delivery system for targeted glioma therapy.* Biomaterials, 2021. **273**: p. 120784.
39. Mehryab, F., et al., *Exosomes as a next-generation drug delivery system: An update on drug loading approaches, characterization, and clinical application challenges.* Acta biomaterialia, 2020. **113**: p. 42-

62.

40. Yang, C., et al., *Desialylated mesenchymal stem cells-derived extracellular vesicles loaded with doxorubicin for targeted inhibition of hepatocellular carcinoma.* Cells, 2022. **11**(17): p. 2642.
41. Wei, H., et al., *A nanodrug consisting of doxorubicin and exosome derived from mesenchymal stem cells for osteosarcoma treatment in vitro.* International journal of nanomedicine, 2019: p. 8603-8610.
42. Qi, H., et al., *Blood exosomes endowed with magnetic and targeting properties for cancer therapy.* ACS nano, 2016. **10**(3): p. 3323-3333.
43. Agrawal, A.K., et al., *Milk-derived exosomes for oral delivery of paclitaxel.* Nanomedicine: Nanotechnology, Biology and Medicine, 2017. **13**(5): p. 1627-1636.
44. Kalani, A., et al., *Curcumin-primed exosomes mitigate endothelial cell dysfunction during hyperhomocysteinemia.* Life sciences, 2014. **107**(1-2): p. 1-7.
45. Mizuta, Y., et al., *Sodium thiosulfate prevents doxorubicin-induced DNA damage and apoptosis in cardiomyocytes in mice.* Life Sciences, 2020. **257**: p. 118074.
46. Chen, J., *The cell-cycle arrest and apoptotic functions of p53 in tumor initiation and progression.* Cold Spring Harbor perspectives in medicine, 2016. **6**(3): p. a026104.
47. Lee, Y.L., et al., *Sirtuin 1 facilitates generation of induced pluripotent stem cells from mouse embryonic fibroblasts through the miR-34a and p53 pathways.* 2012.
48. Jeter, C.R., et al., *Concise review: NANOG in cancer stem cells and tumor development: an update and outstanding questions.* Stem cells, 2015. **33**(8): p. 2381-2390.
49. Ebeid, S.A., et al., *Combination of doxorubicin and berberine generated synergistic anticancer effect on breast cancer cells through down-regulation of NANOG and miRNA-21 gene expression.* Middle East Journal of Cancer, 2020. **11**(3): p. 273-285.
50. Lin, T. and Y. Lin, *p53 switches off pluripotency on differentiation.* Stem cell research & therapy, 2017. **8**(1): p. 1-7.
51. Yoon, C., et al., *PI3K/Akt pathway and Nanog maintain cancer stem cells in sarcomas.* Oncogenesis, 2021. **10**(1): p. 12.
52. Zhou, J.-J., et al., *Knockdown of NANOG enhances chemosensitivity of liver cancer cells to doxorubicin by reducing MDR1 expression.* International Journal of Oncology, 2014. **44**(6): p. 2034-2040.
53. Piegari, E., et al., *MicroRNA-34a regulates doxorubicin-induced cardiotoxicity in rat.* Oncotarget, 2016. **7**(38): p. 62312.
54. Choi, Y.J., et al., *miR-34 miRNAs provide a barrier for somatic cell reprogramming.* Nature cell biology, 2011. **13**(11): p. 1353-1360.
55. Zheng, S.-Z., et al., *MiR-34a overexpression enhances the inhibitory effect of doxorubicin on HepG2 cells.* World journal of gastroenterology, 2019. **25**(22): p. 2752.
56. Marques, S.C., et al., *High miR-34a expression improves response to doxorubicin in diffuse large B-cell lymphoma.* Experimental Hematology, 2016. **44**(4): p. 238-246. e2.

57. Deng, X., et al., *Hyaluronic acid-chitosan nanoparticles for co-delivery of MiR-34a and doxorubicin in therapy against triple negative breast cancer.* Biomaterials, 2014. **35**(14): p. 4333-4344.
58. Sagrillo-Fagundes, L., J. Bienvenue-Pariseault, and C. Vaillancourt, *Melatonin: The smart molecule that differentially modulates autophagy in tumor and normal placental cells.* PloS one, 2019. **14**(1): p. e0202458.

Table 3

Table 3 is not available with this version

Figures

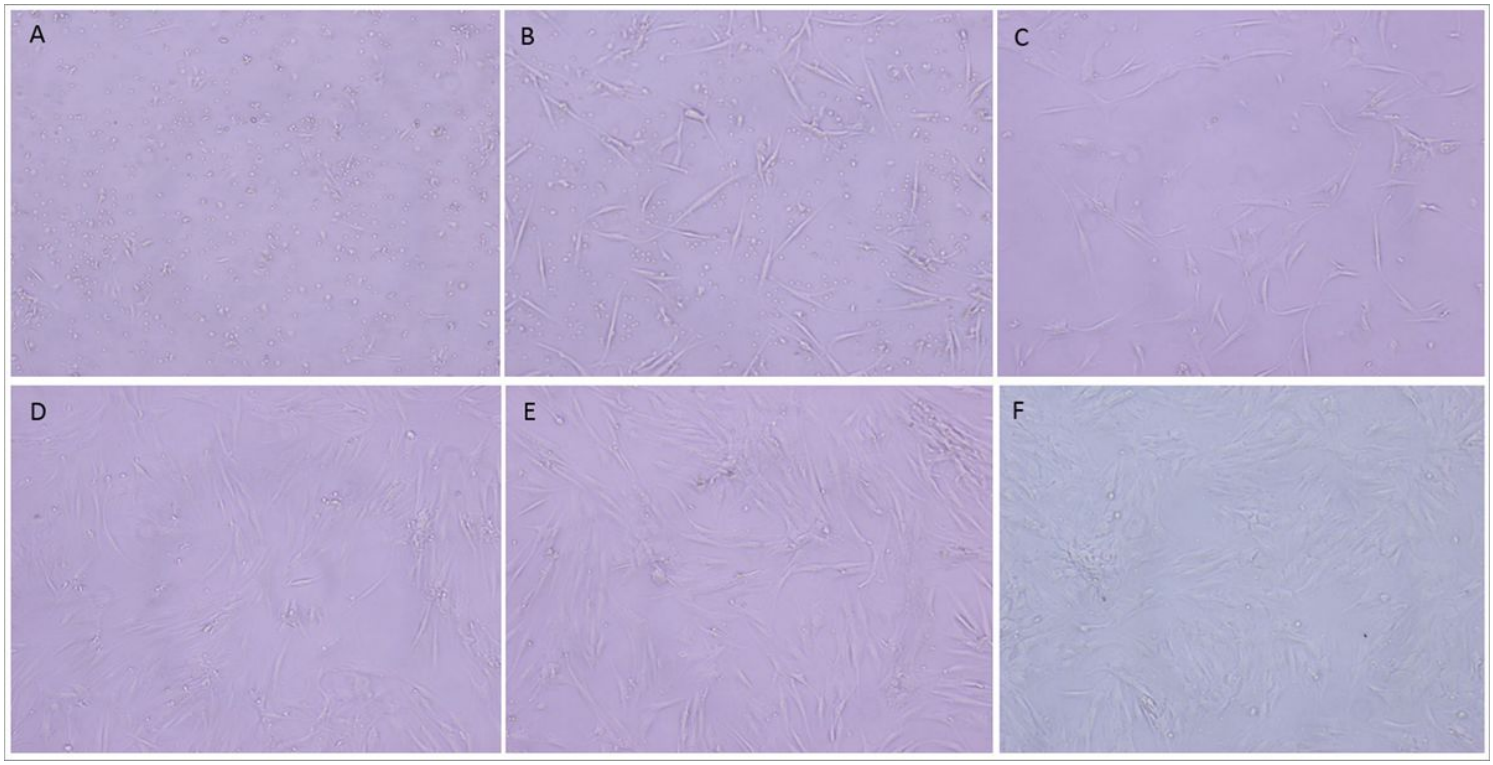

Figure 1

A-MSCs morphology after the separation from adipose tissue in the second day (A), fifth day (B), eighth day (C), first passage (D), second passage (E) and third passage (F).

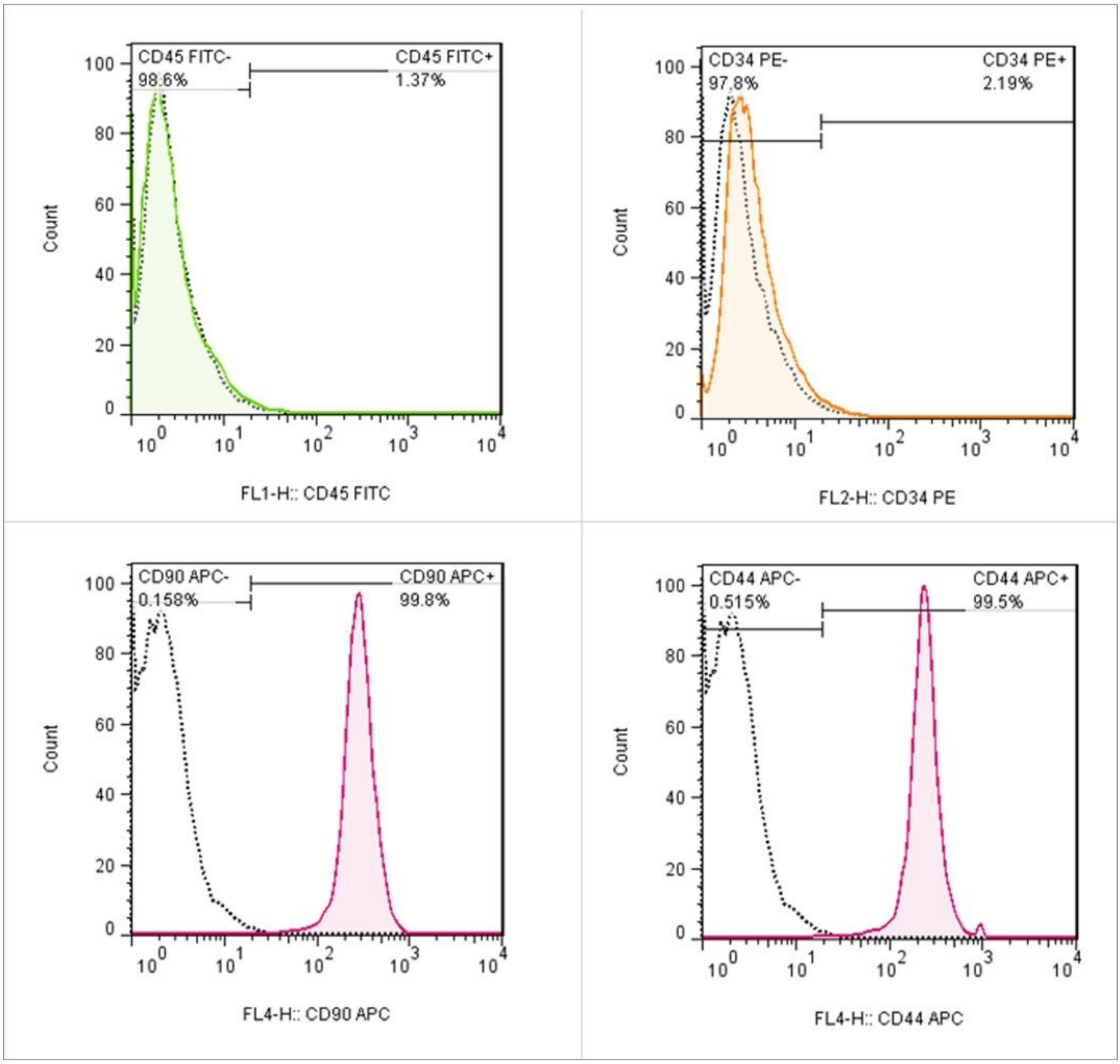

Figure 2

The surface cell markers from A-MSCs. CD45 and CD34 as negative markers, CD44 and CD 90 as positive markers.

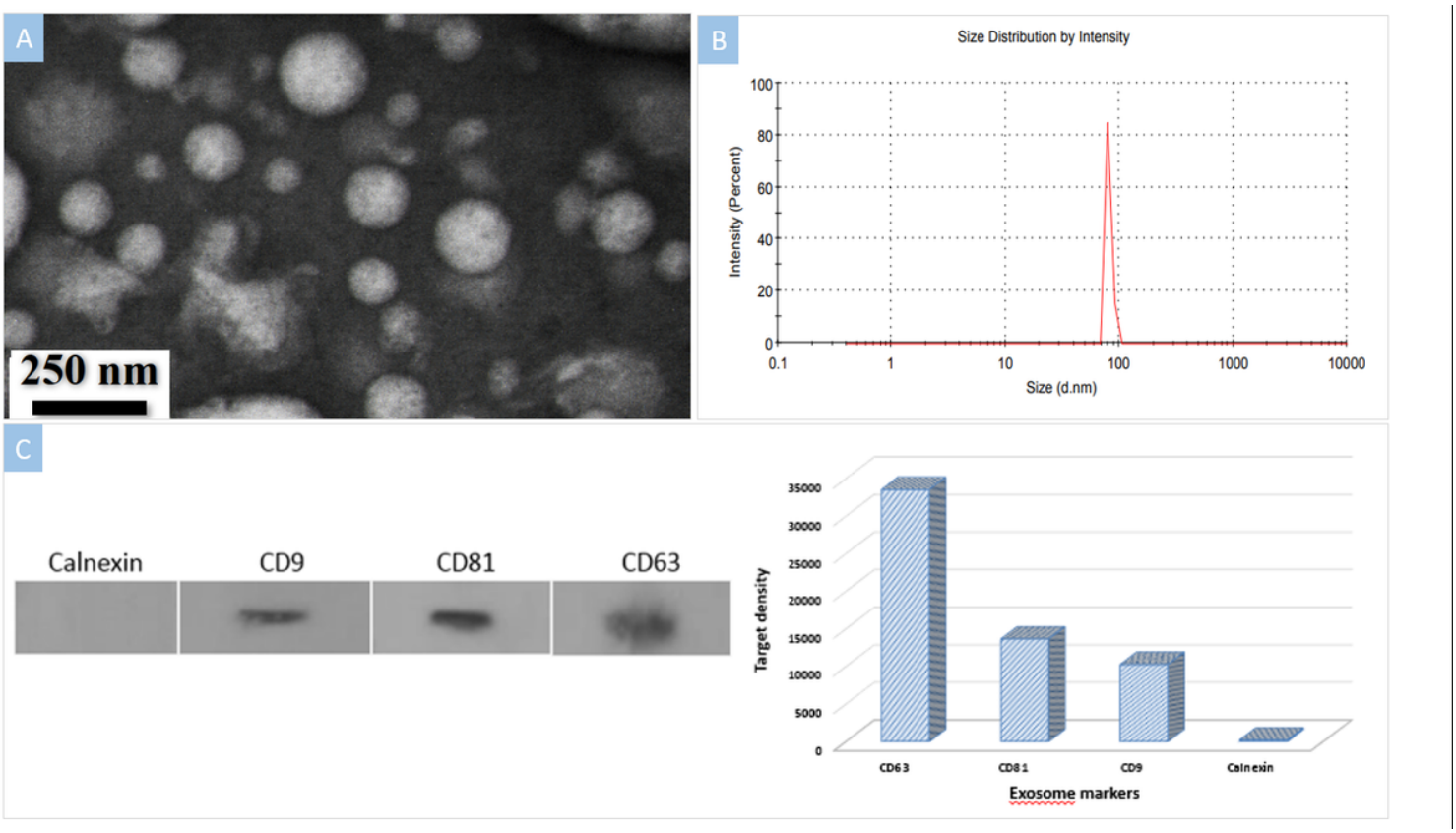

Figure 3

EXOs characterization identified by TEM (A) for morphology, DLS (B) for size and western blot analysis (C) for surface markers.

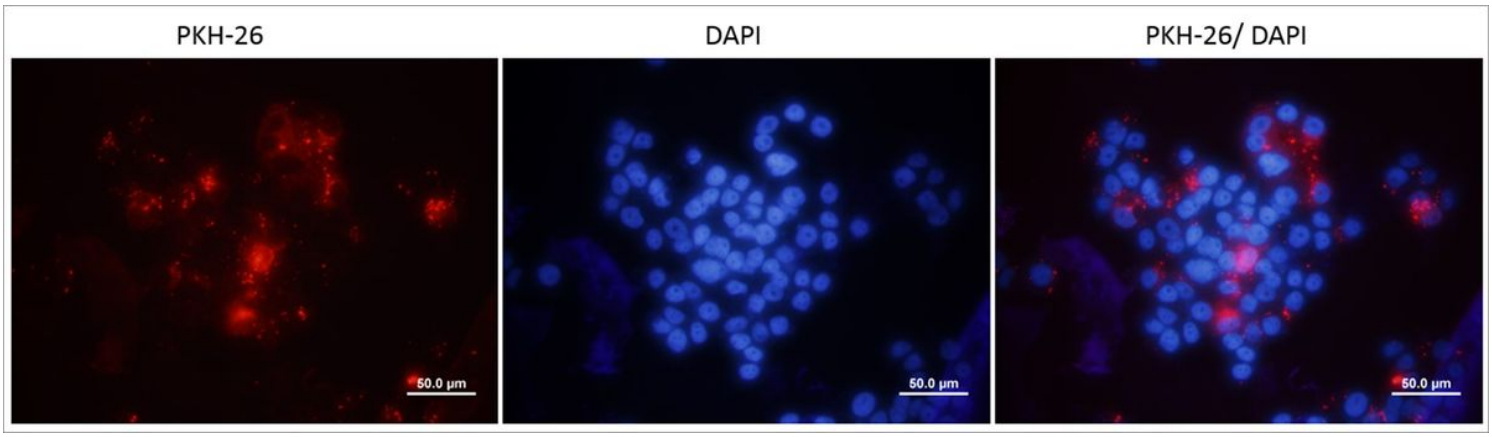

Figure 4

Labeling of EXOs by PKH26 dye and investigation of cellular uptake. Red colors is PKH26 and blue colors is DAPI.

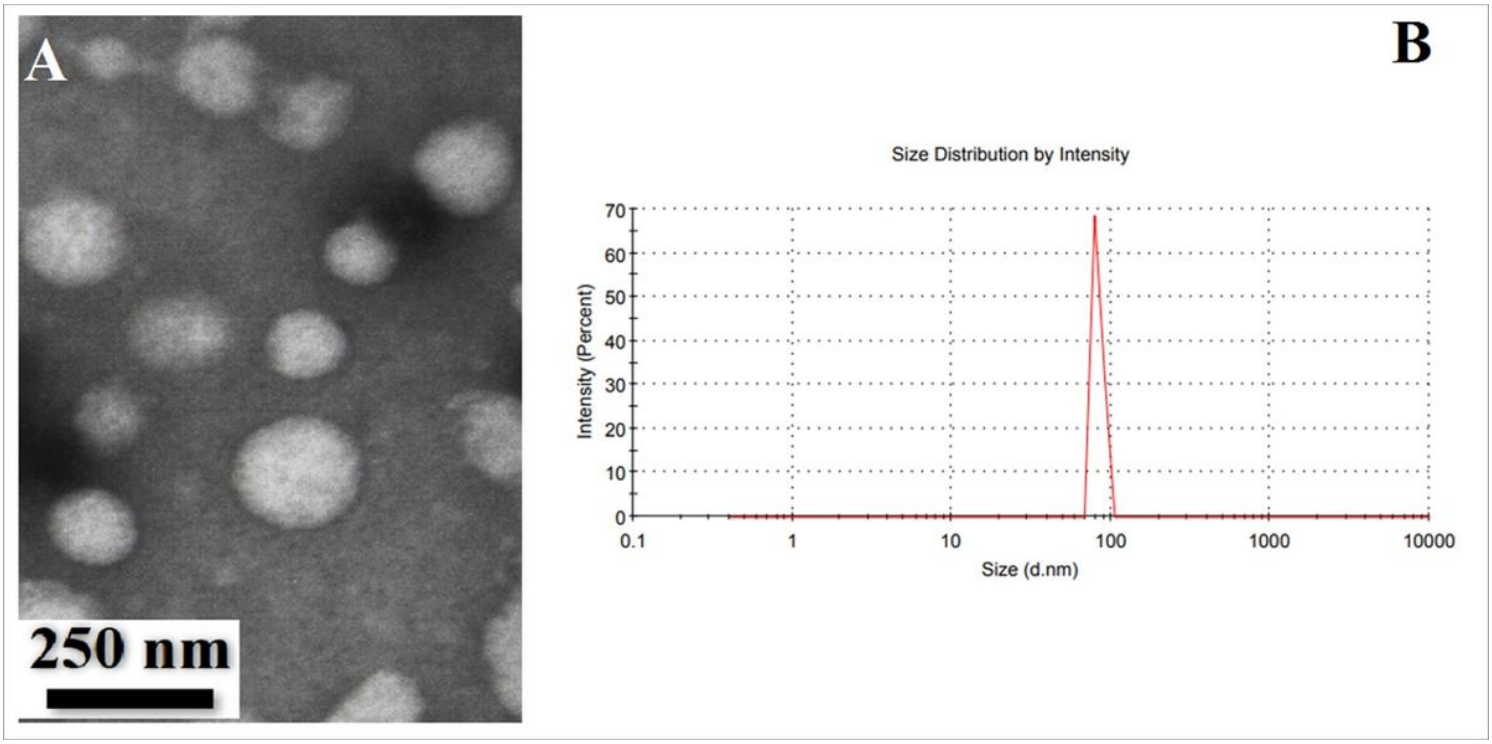

Figure 5

The morphology (A) and size (B) of EXOs after loading drugs by TEM and DLS, respectively.

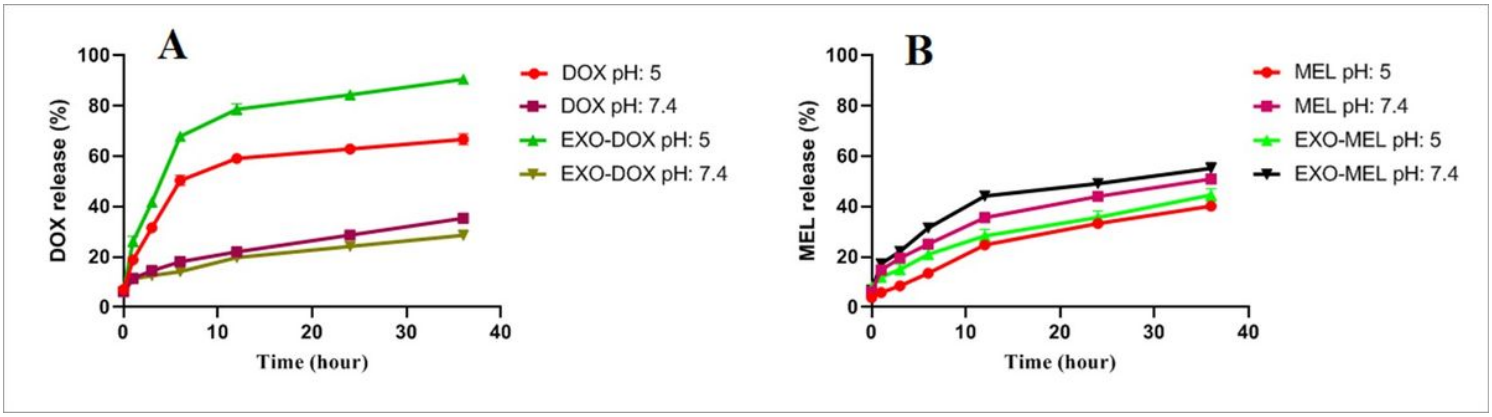

Figure 6

Drug release profile of Exo-Dox (A) and Exo-Mel (B) in PBS with pH 5 and pH 7.4, respectively.

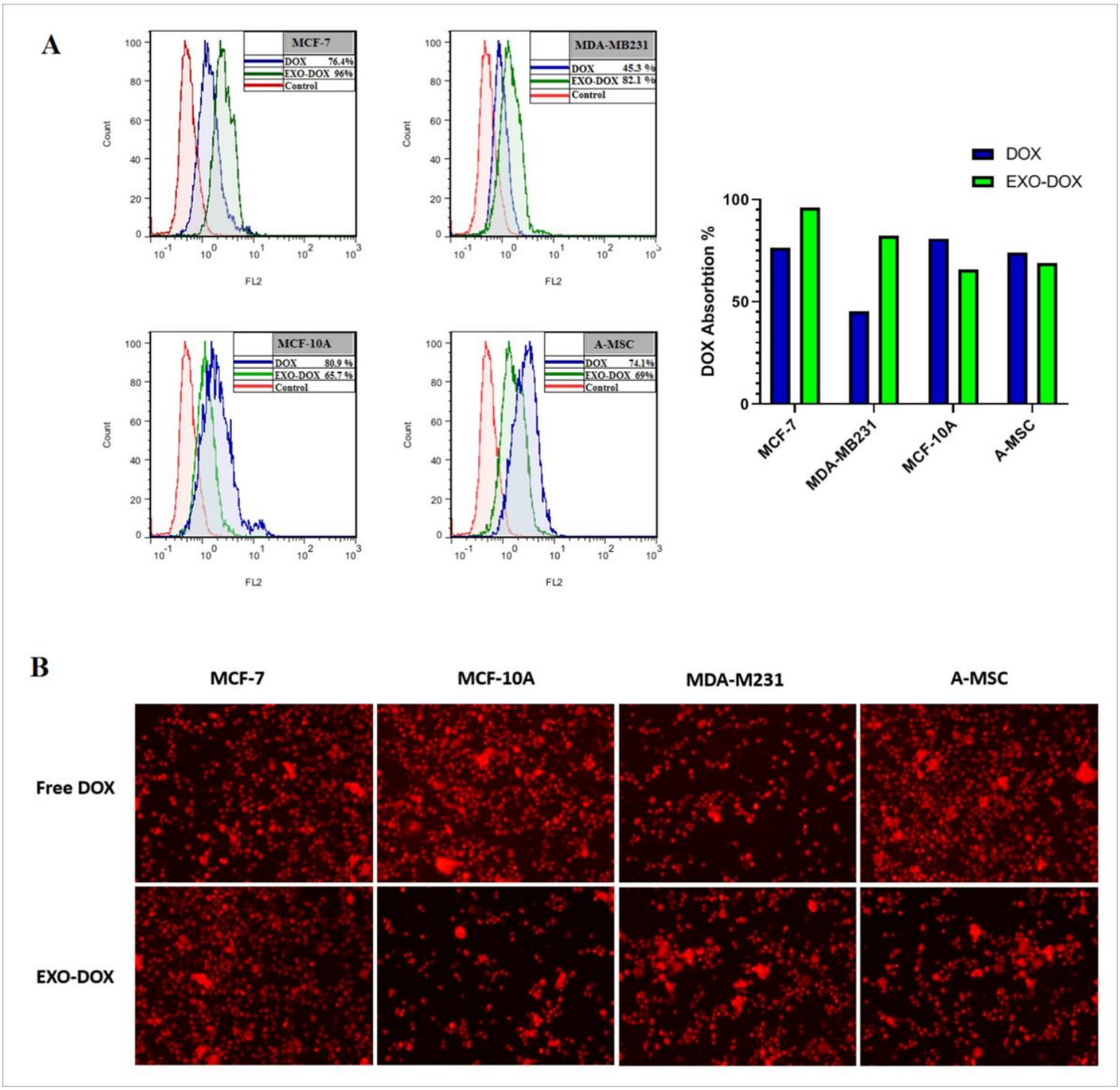

Figure 7

The cellular internalization of the free DOX and Exo-DOX by flow cytometry analysis (A) and fluorescence microscopy (B) in MCF-7, MCF-10A, MDA-MB231, and A-MSC cells after 4 h.

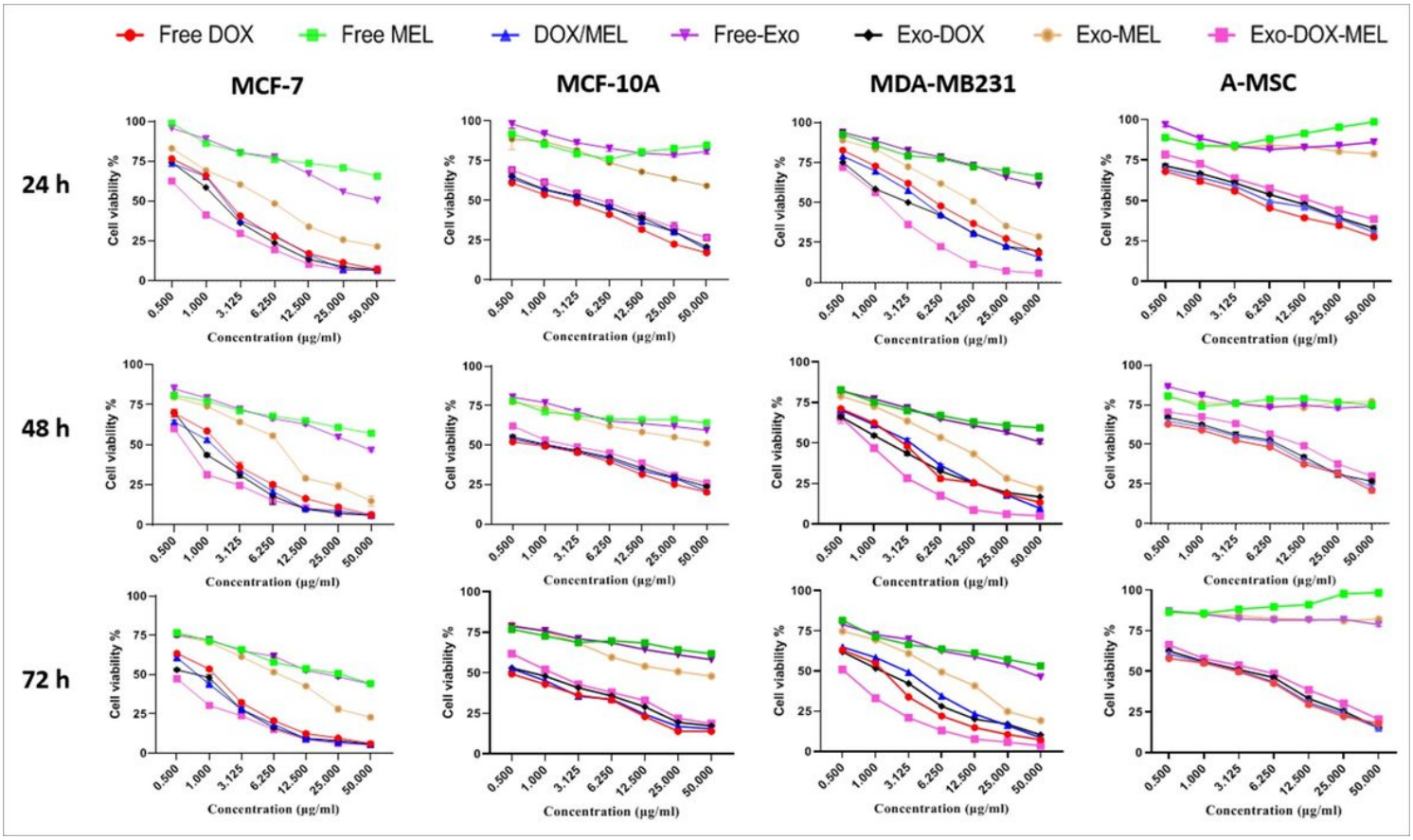

Figure 8

Cytotoxicity effect of free-DOX, free-MEL, DOX/MEL, free-Exo, Exo-DOX, Exo-MEL, and Exo-DOX-MEL on the MCF-7, MDA-MB231, MCF-10A and AMSC cells at 24, 48, and 72 h.

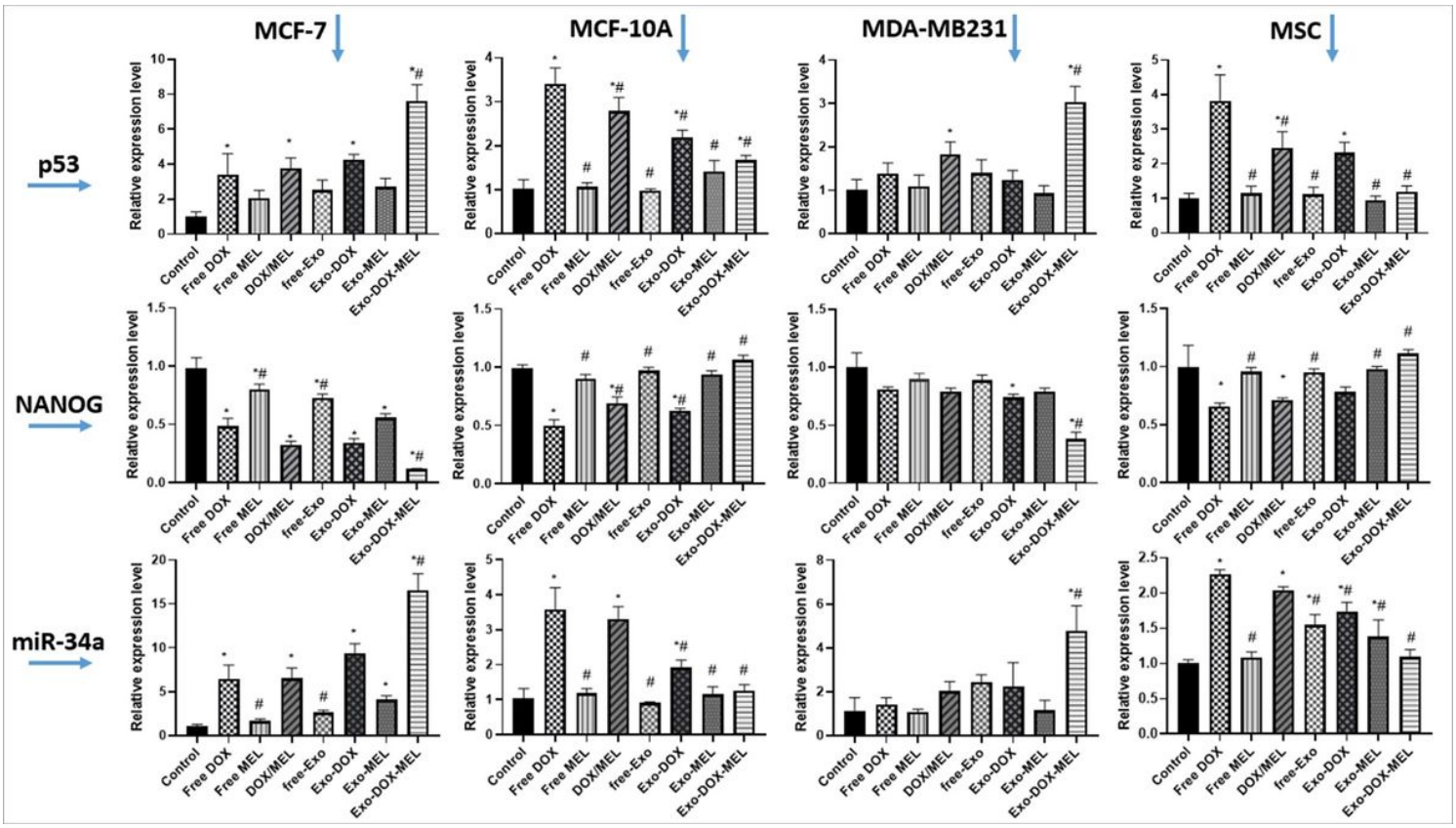

Figure 9

The quantitative real-time RT-PCR analysis. The effects of free-DOX, free-MEL, DOX/MEL, free-Exo, Exo-DOX, Exo-MEL, and Exo-DOX-MEL on expression levels of p53, NANOG, and miR-34a in MCF-7, MDA-MB231, MCF-10A and AMS cell lines. * Comparison with control (no treatment), # Comparison with free-DOX

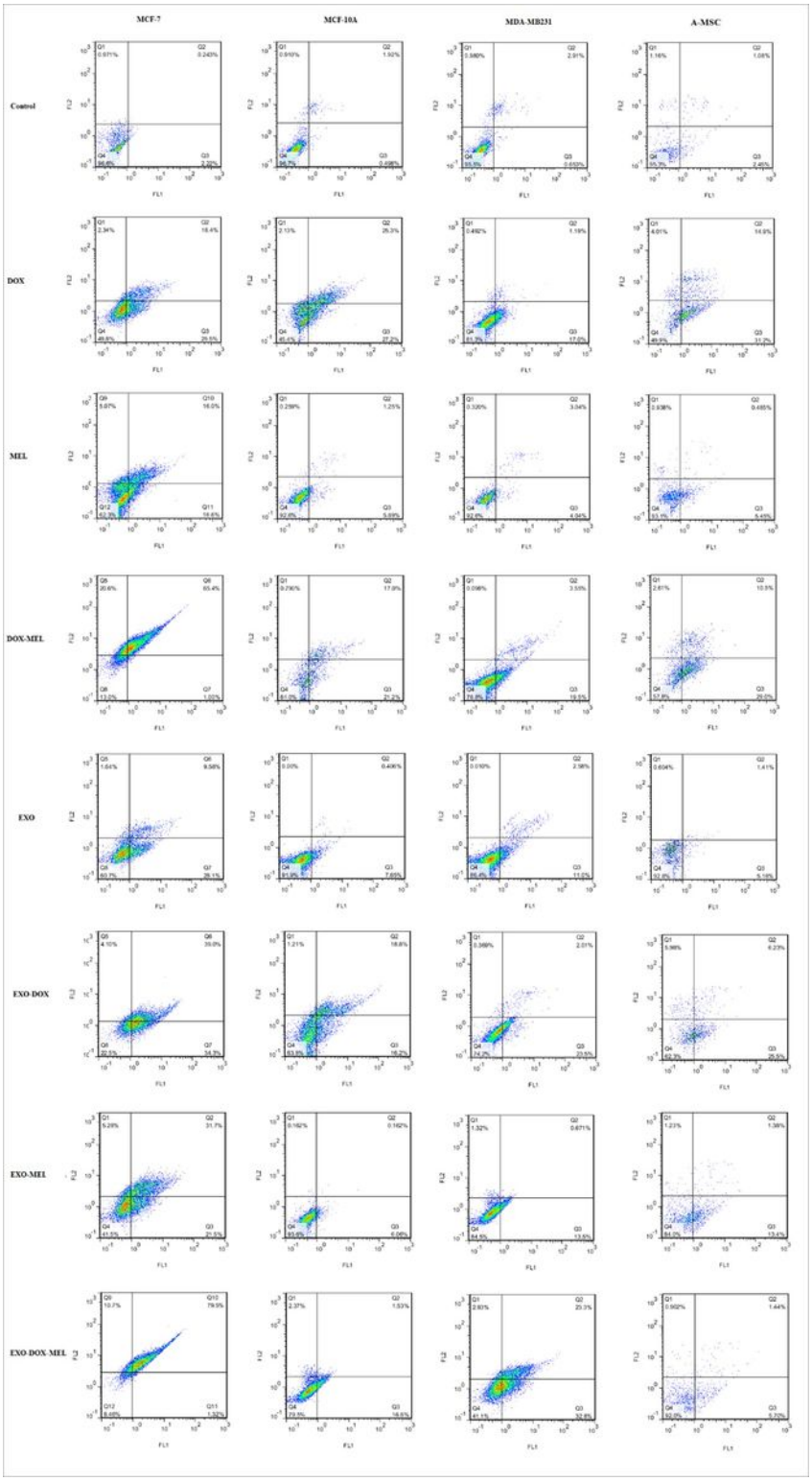

Figure 10

The apoptotic activity of free-DOX, free-MEL, DOX/MEL, free-Exo, Exo-DOX, Exo-MEL, and Exo-DOX-MEL by flow cytometry in MCF-7, MDA-MB231, MCF-10A and AMSC cell lines.

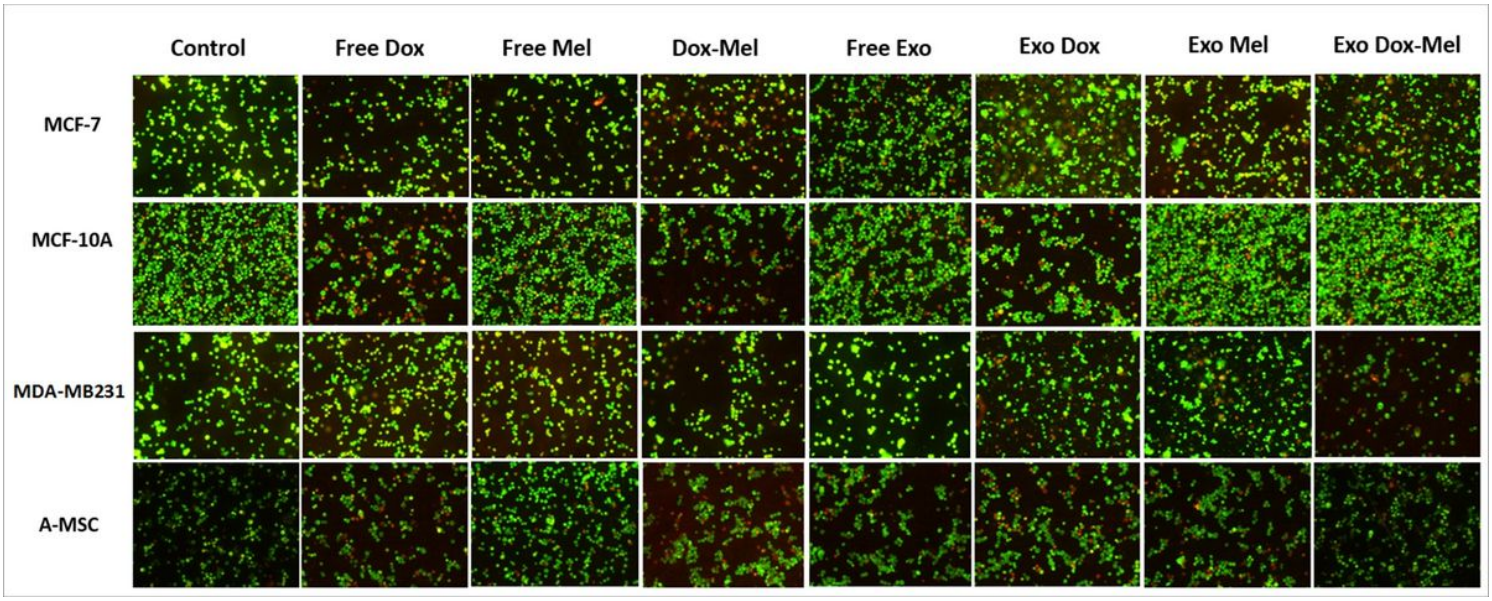

Figure 11

Acridine orange/ethidium bromide staining of morphological analysis of cells exposed to different drugs. Green fluorescent cells indicate healthy endothelial cells and red fluorescent cells indicate apoptotic endothelial cells.

Supplementary Files

This is a list of supplementary files associated with this preprint. Click to download.

- GraficalAbstract7.tif